ACS APPLIED MATERIALS & INTERFACES

Letter

www.acsami.org

Open Access on 07/16/2015

Glutathione-Coated Luminescent Gold Nanoparticles: A Surface Ligand for Minimizing Serum Protein Adsorption

Rodrigo D. Vinluan, III,[†] Jinbin Liu,[†] Chen Zhou,[†] Mengxiao Yu,[†] Shengyang Yang,[†] Amit Kumar,[‡] Shasha Sun,[†] Andrew Dean,[†] Xiankai Sun,[‡] and Jie Zheng*[,†]

[†]Department of Chemistry, The University of Texas at Dallas, Richardson, Texas 75080, United States

[‡]Department of Radiology, The University of Texas Southwestern Medical Center, Dallas, Texas 75390 United States

Supporting Information

ABSTRACT: Ultrasmall glutathione-coated luminescent gold nanoparticles (GS-AuNPs) are known for their high resistance to serum protein adsorption. Our studies show that these NPs can serve as surface ligands to significantly enhance the physiological stability and lower the serum protein adsorption of superparamagnetic iron oxide nanoparticles (SPIONs), in addition to rendering the NPs the luminescence property. After the incorporation of GS-AuNPs onto the surface of SPIONs to form the hybrid nanoparticles (HBNPs), these SPIONs' protein adsorption was about 10-fold lower than those of the pure glutathione-coated SPIONs suggesting that GS-AuNPs are capable of providing a stealth effect against serum proteins.

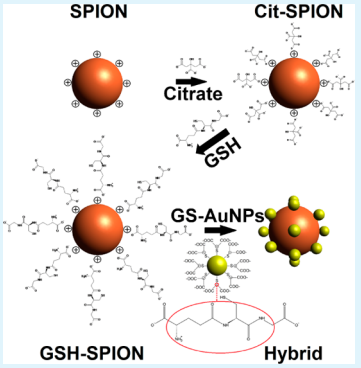

KEYWORDS: *luminescent gold nanoparticles, iron oxide, integrated, hybrid nanoparticles*

Surface passivation with small organic ligands or polymers is one of the most common strategies to enhance physiological stabilities of inorganic nanoparticles (NPs) and minimize their nonspecific binding to serum proteins. For example, Choi et al. found that coating quantum dots (QDs) with small zwitterionic cysteine ligand not only made QDs highly stable in a native physiological environment, but also enhanced their resistance to serum protein adsorption.[1] Coating gold NPs (AuNPs) with glutathione (GSH), a triamino acid peptide, also leads to a class of renal clearable AuNPs with high resistance to serum protein adsorption that can effectively target tumors.[2,3] Not limited to small molecules, polymers such as polyethylene glycol (PEG) can also enhance their physiological stability.[4,5] For instance, PEGylation renders gold nanocages highly stable in a physiological environment with efficient tumor targeting.[6] In addition, coating QDs and AuNPs with low-molecular-weight PEGs leads to a class of inorganic NPs that have little affinity to serum proteins and can effectively target tumors at high efficiency.[7,8]

Although these organic ligands have been widely used to stabilize inorganic NPs in the physiological environment, they seldom render the NPs new functionalities that often need to be achieved by integrating distinct nanostructures together. For instance, a variety of metal and magnetic NPs have been fused to develop hybrid NPs for multimodality imaging that allow strengths of different imaging techniques to be integrated for better healthcare management.[9−16] However, hybridizing different NPs together into a single unit or entity often suffers from significantly increased overall size and decreased physiological stability, which limits their potential in vivo application.[17] Herein, we report a proof-of-concept strategy to address this challenge. By using GSH coated luminescent AuNPs as surface ligands to decorate SPIONs, not only can we successfully integrate magnetic and fluorescence properties together, but also significantly enhance the hybrid nanoparticles (HBNPs) physiological stability and minimize serum protein adsorption, opening up a new path to develop multimodality contrast agents with enhanced physiological behaviors.

The GSH-coated SPIONs were obtained through a two-step process: (1) coating with citrate and (2) replacement of the citrate by GSH. Briefly, 2 nm luminescent GS-AuNPs are fabricated using a method similar to our previously published work.[18] The SPIONs are synthesized via a coprecipitation method by addition of a base to a salt solution containing Fe^{2+} and Fe^{3+} to form magnetite (Fe_3O_4), followed by its oxidation into SPIONs (γ-$F_{e2}O_3$). The stepwise procedure reported by Kang et al. was adopted with slight modifications.[19] These SPIONs were initially coated with citrate, which were then replaced with GSH to act as linkers between the SPIONs and ∼2 nm luminescent GS-AuNPs to form the HBNPs. The thiol (−SH) group of glutathione in GSH-SPIONs bonds strongly with the GS-AuNPs, whereas the negatively charged carboxylic ends of the GS-AuNPs can coordinate with the GSH-SPIONs' surface.[20]

Received: May 20, 2014
Accepted: July 16, 2014
Published: July 16, 2014

Transmission electron microscopy (TEM) and particle size analyzer dynamic light scattering (DLS) were used to validate the assembly of the integrated NPs, as well as determine their core size and hydrodynamic diameter (HD). The morphology and particle size distribution of the GSH-SPIONs and HBNPs are shown in Figure 1. Because Au is naturally more electron-

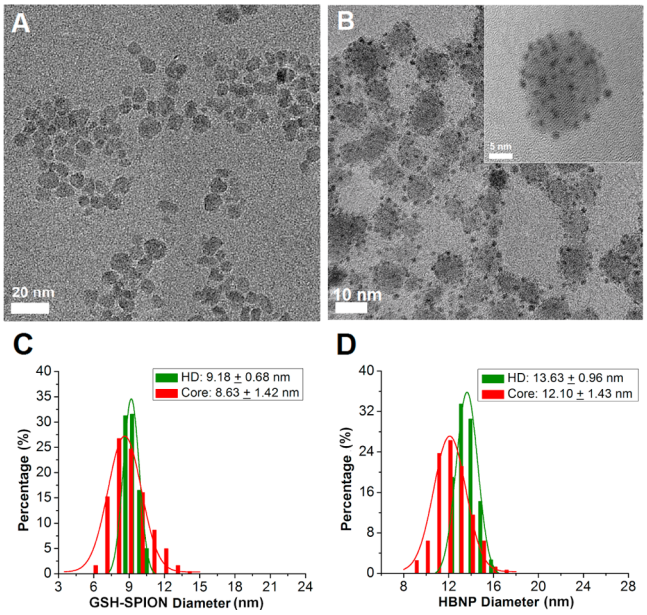

Figure 1. TEM images of (A) GSH-SPIONs and (B) HBNPs in H_2O showing their size and morphology. HD and core size distribution of (C) GSH-SPIONs and (D) HBNPs.

dense than Fe, fewer electrons are transmitted, making the GS-AuNPs easily distinguishable and appear darker than the GSH-SPIONs in the TEM images.[13] As illustrated in Figure 1, there are no observable free GS-AuNPs, indicating that the purified solution consists solely of HBNPs. Several additional TEM images of the HBNPs (n = 20) were analyzed to quantify the number of GS-AuNPs bound to the surface of each SPION and determined that there are 15 ± 3.5 GS-AuNPs on average for each ~12 nm HBNP, a value that is dependent on the size and surface area of the SPIONs (see Figure S2 in the Supporting Information). Using DLS, the size distribution of the SPIONs (see Figure S3 in the Supporting Information) shows no significant change after the citrate ligands were replaced by GSH (9.03 ± 0.62 nm to 9.18 ± 0.68 nm). However, the incorporation of GS-AuNPs onto the surface of ~9 nm GSH-SPIONs, resulted in the increase of the overall core and HD size to 12.10 ± 1.43 nm and 13.63 ± 0.96 nm, respectively (Figure 1C, D). This change in size is an indication that the GS-AuNPs were successfully integrated onto the SPIONs' surface. In addition, the zeta potential (ζ) was measured to determine the surface charge. The surface of the hydroxyl-functionalized SPIONs (bare-SPIONs) is positively charged as determined by its ζ value of 35.12 ± 0.75 mV. On the other hand, the citrate-coated SPIONs, GSH-SPIONs, and HBNPs, all have negative ζ potential (−58.34 ± 1.44 mV, −46.27 ± 2.50 mV, and −48.30 ± 0.67 mV, respectively) under physiological pH (pH 7.4). The transition in the ζ potential from positive to negative indicates that the bare SPIONs were successfully coated with ligands. Chemically, these ligands have more negatively charged carboxyl groups than GSH, which is in agreement with their ζ potential measurements. Moreover, the overall surface charge of the HBNPs is more negative than the GSH-SPIONs because of the incorporation of multiple GS-AuNPs on the surface.

The ligands on the surface of the NPs were characterized using Fourier Transform Infrared spectroscopy (FTIR) to acquire and confirm their chemical composition and structure, as shown in Figure 2. The spectrum of the citrate-SPIONs

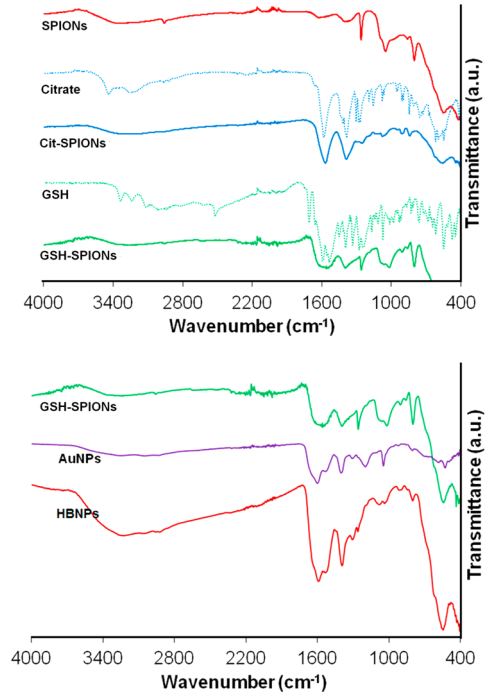

Figure 2. FTIR spectra of the superparamagnetic SPIONs (coated with different ligands), AuNPs, and the HBNPs.

shows the emergence of the signature peaks from the citrate, which come from the symmetric and asymmetric stretching vibrations of the carboxylate moiety that appear at 1387 and 1568 cm^{-1}, respectively. Aside from its similarities with the IR spectrum of citrate, the result obtained here is in accordance with previously published data.[21] The spectrum of GSH-SPIONs also shows a peak around 1600 cm^{-1} (characteristic peak of −COOH groups), but not as sharp as that for GSH. The spectrum of the HBNPs is analogous to that of the GS-AuNPs due to the presence of GSH ligands on their surface. The peak observed at 2520 cm^{-1} for GSH (attributed to the presence of −SH group), is absent in the spectrum of AuNPs and HBNPs because of the formation of a strong Au-thiol bond. In GSH-SPIONs, the 2520 cm^{-1} peak is also absent, which may be due to the development of disulfide bonds.[22] The peak detected at about 560−580 cm^{-1} for all of the SPIONs in Figure 2 corresponds to the Fe−O bond vibrations.[23]

The photoluminescence and magnetic properties before and after exposure to a magnet and UV light are shown in Figure 3. To quantify the differences in the properties, we used an inductively coupled plasma mass spectrometer (ICP-MS) to determine the concentration of gold and iron in the AuNPs and HBNPs, since it is difficult to distinguish the two via UV−vis spectroscopy due to an absorption overlap from 300 to 450 nm (Figure 3B). According to the ICP-MS analysis (see Figure S4 in the Supporting Information), the HBNP solution contains approximately 4.15 mM Au (~15% by weight) and 84.09 mM

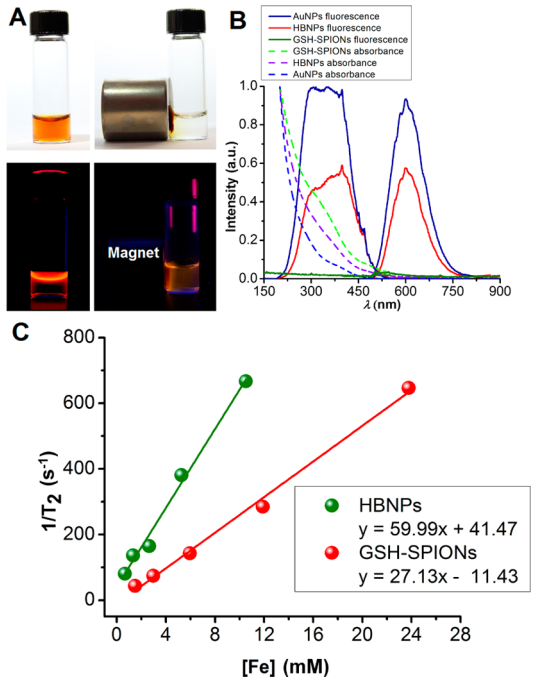

Figure 3. (A)HBNP solution before and after exposure to UV light and magnet, (B) fluorescence with UV–vis spectra of GSH-SPIONs, GS-AuNPs, and hybrid nanostructures in H_2O, and (C) T_2 relaxivities of HBNPs and GSH-SPIONs.

Fe (~85%), whereas the GS-AuNP solution contains 5.37 mM Au. This result enabled us to quantitatively compare the fluorescence (FL) of the HBNPs with that of the GS-AuNPs. Both the GS-AuNPs and the HBNPs have the same excitation and emission wavelengths at 400 and 600 nm, respectively. The solution of GS-AuNPs has almost double the FL intensity than that of the HBNPs measured at similar Au concentration, whereas the GSH-SPIONs are nonfluorescent. To quantify the FL quenching mechanism of HBNPs, the quantum yield (QY) was determined by comparing the NPs' FL and absorbance with Rhodamine 6G's (R6G), which has a known QY of 90% in water.[24] As shown in Figure S5 in the Supporting Information, the QY of the HBNPs was 1.36%, compared to the GS-AuNPs' 4.25%. This decrease in the luminescence of the HBNPs may be attributed to self-quenching of photoluminescence from the AuNPs due to their short distances from one another, as well as potential electron transfer between luminescent AuNPs and SPIONs.[25−27]

Using a Vibrating Sample Magnetometer (VSM) with an applied magnetic field from −10 kOe to 10 kOe at 298 K, the magnetic properties of plain GSH-SPIONs and HBNPs were characterized and shown in Figure S6 in the Supporting Information, which indicates that the NPs are superparamagnetic at room temperature, showing no coercivity and remanence as also observed in Au BSA modified DOPFe (HQC).[15] The GSH-SPIONs exhibit a mass magnetization (M_s) of ~50 emu/g, a value that is ~2 times greater than what was previously reported for SPIONs.[28,29] On the other hand, the GS-AuNPs do show no response to the applied field, an expected typical diamagnetic behavior. The HBNP contains ~15% gold by weight as determined by ICP-MS, and after taking into account the mass contributed by the GS-AuNPs, the M_s of HBNP is measured as ~40 emu/g (~35 emu/g before normalization), which is comparable to those of the plain GSH-SPIONs but slightly lower than those of magnetism-engineered iron oxide (MEIO) NPs with similar diameter.[30] The spin−spin relaxation times (T_2) were also evaluated for the GSH-SPIONs and HBNPs at different iron concentrations (0.66 mM to 23.77 mM). The inverse of the T_2 relaxation time ($1/T_2$) was plotted against iron concentration, and the relaxivity coefficient (r_2) calculations reveal that the HBNPs (59.99 mM^{-1} s^{-1}) have a higher r_2 value than the GSH-SPIONs (27.13 mM^{-1} s^{-1}) as shown in Figure 3C. Because the r_2 relaxivity of magnetic nanoparticles (MNPs) is determined by the translational diffusion of water molecules in the inhomogeneous magnetic field around the NPs, the surface coatings have a significant influence on their relaxivity.[31] For example, when the molecular weight of PEG used to coat the surface of a 14 nm iron oxide nanoparticle (IONP) decreased from 5000 to 1000 Da, the relaxivity increased almost 3 times.[32] This phenomenon is also observed in silica-coated MNPs.[33] The r_1 values of the MNPs increased with the silica interlayer thickness, whereas the r_2 values decreased. These results show that modifying the IONPs' surface has an impact on relaxivity. Nevertheless, the r_2 values of HBNPs, which are a direct indication of contrast enhancement effects, are comparable to those of dextran-coated monocrystalline IONPs and Clariscan (a superparamagnetic IONP) that have similar core diameters (~9 nm @ 43.7 mM^{-1} s^{-1} and ~7 nm @ 35 mM^{-1} s^{-1}), making the HBNPs a promising candidate for magnetic resonance imaging (MRI).[32]

The in vitro stability of these hybrid nanostructures was also investigated in phosphate buffered saline (PBS) buffer and fetal bovine serum (FBS) and compared them with GSH-SPIONs. As shown in Figure 4, the HD of HBNPs in PBS is 12.82 ± 0.99 nm and increased to 18.02 ± 2.12 nm when incubated in PBS containing 10% FBS. However, these HD values are still much smaller than those of plain GSH-SPIONs (9.18 ± 0.68 nm in H_2O, 50.79 ± 4.86 nm in PBS, and 110.54 ± 12.26 nm in PBS with 10% FBS), as observed in a recently published data.[22] Combined with our previous work that GS-AuNPs have high resistance to serum protein adsorption,[16] significant

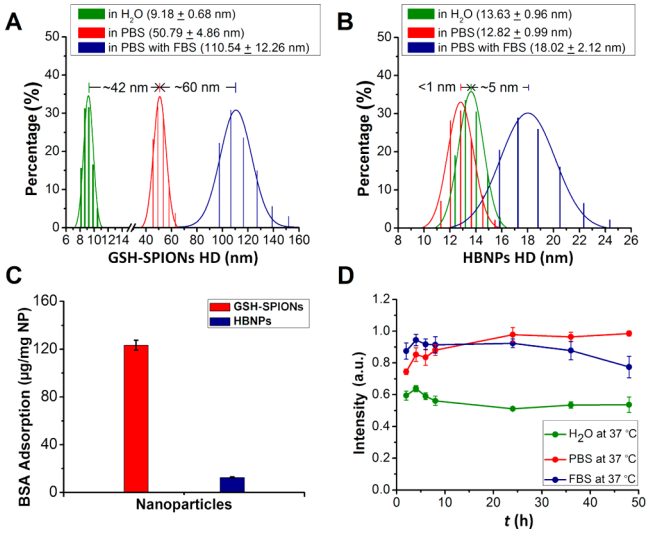

Figure 4. Stability of the HBNPs in different solutions. HD of (A) GSH-SPIONs compared to (B) HBNPs in PBS after 1 h incubation (red) and in PBS with 10% FBS (blue). (C) Bradford protein assay showing the quantitative data of serum protein adsorption. (D) Fluorescence intensity of the HBNPs at 37 °C.

dx.doi.org/10.1021/am5031374 | ACS Appl. Mater. Interfaces 2014, 6, 11829−11833

differences in HDs between HBNPs and plain GSH-SPIONs suggest that incorporating GS-AuNPs into the SPIONs not only allows integration of fluorescence and magnetic properties, but also significantly enhances their resistance to serum protein adsorption. The presence of divalent cations such as Mg^{2+} in PBS buffer is believed to cause aggregation of GSH-SPIONs in PBS, because of the formation of a cation salt bridge between two carboxylic groups.[22] As shown in Figure S7B, C in the Supporting Information, the HD of GSH-SPIONs increased to ~140 nm in a solution containing 250 μM of Mg^{2+}, whereas the HD of HBNPs only increased to ~40 nm after 1 h of incubation at room temperature. This is important because the human serum has a normal magnesium concentration that ranges from 0.65 to 1.05 mM, in which 55−70% of it comes in ionized form.[34] The HBNPs and GSH-SPIONs were also incubated in sodium chloride (NaCl) solutions for 1 h to determine their stability. As shown in Figure S7C in the Supporting Information, both types of NPs are stable in different NaCl concentrations, as also observed in a similar study for GSH-coated iron oxide nanoparticles that was reported recently.[22] In the presence of serum proteins (10% FBS in PBS), the GSH-SPIONs' HD increased to ~110 nm compared to the HD in PBS (~50 nm), indicating that serum protein adsorption caused the particles to aggregate even more. On the other hand, the HBNPs' increased HD in the presence of serum proteins is believed to be due to slight adsorption. Although individual GS-AuNPs have been shown to have a stealth effect against serum proteins, the GS-AuNPs in HBNPs are sparsely distributed with a relatively small distance between the GS-AuNPs (2.8 ± 0.7 nm), as shown in Figure S9 in the Supporting Information. This distance might make serum proteins in FBS (which have an average HD of 5−10 nm)[35] more difficult to adsorb on the SPION core; therefore, only a slight increase in the HBNPs' HD in 10% FBS was observed. Therefore, Bradford protein assay was used to quantify the amount of proteins adsorbed on the nanoparticles, where bovine serum albumin (BSA) was used as the standard. As shown in Figure 4C, ~120 μg/mg NP of BSA was adsorbed by GSH-SPIONs after 1 h of incubation, whereas the HBNPs only adsorbed ~15 μg/mg NP of BSA, which further proves that GS-AuNPs can minimize the serum protein adsorption. The additional TEM studies on the HBNPs after serum protein incubation show that the number of GS-AuNPs on the surface of SPION after 48 h of incubation in PBS with 10% FBS was 14 ± 3, which is comparable to the number of 15 ± 3.5 in H_2O (see Figure S2 in the Supporting Information). In addition, the HBNPs' FL stability was monitored over a 48 h period, after incubation in H_2O, PBS, and 10% FBS in PBS at R.T. and 37 °C, respectively. Figure 4D shows no significant change in the nanostructures' FL intensity, even in the presence of serum proteins (10% FBS). At 37 °C, the FL intensity of the particles incubated in PBS remained constant, indicating their high stability. Compared to the luminescence intensity in H_2O, there is a slight increase in PBS because of a difference in pH. However, in PBS containing 10% FBS at 37 °C, the intensity slightly decreased by about 10%, which may be due to the interactions with proteins as indicated by a small increase in the HD from 12.82 ± 0.99 to 18.02 ± 2.12 nm for the HBNPs and the protein assay (Figure 4A, C, respectively).

In summary, ultrasmall luminescent GS-AuNPs with high resistance to serum protein adsorption can serve as surface ligands to stabilize SPIONs, which not only render SPIONs fluorescence property but also enhance their physiological stability, and minimize serum protein adsorption 10 times lower than the SPIONs coated with only GSH. These unique functionalities of ultrasmall luminescent GS-AuNPs can potentially enhance the in vivo behavior of SPIONs, opening up a new strategy for designing multimodal imaging probes with enhanced functionalities and physiological stabilities. With the assistance of dual-functionalities of these hybrid nanostructures, the deep penetration depth of MRI can be integrated with high sensitivity of fluorescence imaging, so that both preoperative planning and surgery can be more accurately coordinated to further improve the effectiveness in radical resection.

■ ASSOCIATED CONTENT

Ⓢ Supporting Information

Experimental section, as well as supplementary figures. This material is available free of charge via the Internet at http://pubs.acs.org.

■ AUTHOR INFORMATION

Corresponding Author

*Tel.: 972-883-5768. Fax: 972-883-2925. E-mail: jiezheng@utdallas.edu.

Author Contributions

The manuscript was written through contributions of all authors. All authors have given approval to the final version of the manuscript.

Notes

The authors declare no competing financial interest.

■ ACKNOWLEDGMENTS

This work was supported in part by the NIH (1R21EB011762), CPRIT (RP120588), and the start-up fund from The University of Texas at Dallas (J.Z.).

■ ABBREVIATIONS

PEG, polyethylene glycol
QD, quantum dot
NP, nanoparticle
GSH, glutathione
AuNP, gold nanoparticle
SPION, superparamagnetic iron oxide nanoparticle
HBNP, hybrid nanoparticle
FL, fluorescence
VSM, vibrating sample magnetometer
MNP, magnetic nanoparticle
TEM, transmission electron microscopy
DLS, dynamic light scattering
HD, hydrodynamic diameter
PBS, phosphate buffer saline
FBS, fetal bovine serum

■ REFERENCES

(1) Soo Choi, H.; Liu, W.; Misra, P.; Tanaka, E.; Zimmer, J. P.; Itty Ipe, B.; Bawendi, M. G.; Frangioni, J. V. Renal Clearance of Quantum Dots. *Nat. Biotechnol.* **2007**, *25*, 1165−1170.

(2) Liu, J.; Yu, M.; Zhou, C.; Yang, S.; Ning, X.; Zheng, J. Passive Tumor Targeting of Renal-Clearable Luminescent Gold Nanoparticles: Long Tumor Retention and Fast Normal Tissue Clearance. *J. Am. Chem. Soc.* **2013**, *135*, 4978−4981.

(3) Zhou, C.; Long, M.; Qin, Y.; Sun, X.; Zheng, J. Luminescent Gold Nanoparticles with Efficient Renal Clearance. *Angew. Chem., Int. Ed.* **2011**, *50*, 3168−3172.

(4) Kim, J.; Kim, H. S.; Lee, N.; Kim, T.; Kim, H.; Yu, T.; Song, I. C.; Moon, W. K.; Hyeon, T. Multifunctional Uniform Nanoparticles Composed of a Magnetite Nanocrystal Core and a Mesoporous Silica Shell for Magnetic Resonance and Fluorescence Imaging and for Drug Delivery. *Angew. Chem., Int. Ed.* **2008**, *47*, 8438−8441.
(5) Larsen, E. K. U.; Nielsen, T.; Wittenborn, T.; Birkedal, H.; Vorup-Jensen, T.; Jakobsen, M. H.; Østergaard, L.; Horsman, M. R.; Besenbacher, F.; Howard, K. A.; Kjems, J. Size-Dependent Accumulation of PEGylated Silane-Coated Magnetic Iron Oxide Nanoparticles in Murine Tumors. *ACS Nano* **2009**, *3*, 1947−1951.
(6) Wang, Y.; Liu, Y.; Luehmann, H.; Xia, X.; Brown, P.; Jarreau, C.; Welch, M.; Xia, Y. Evaluating the Pharmacokinetics and In Vivo Cancer Targeting Capability of Au Nanocages by Positron Emission Tomography Imaging. *ACS Nano* **2012**, *6*, 5880−5888.
(7) Liu, J.; Yu, M.; Ning, X.; Zhou, C.; Yang, S.; Zheng, J. PEGylation and Zwitterionization: Pros and Cons in the Renal Clearance and Tumor Targeting of Near-IR-Emitting Gold Nanoparticles. *Angew. Chem., Int. Ed.* **2013**, *52*, 12572−12576.
(8) Matsumura, Y.; Maeda, H. A New Concept for Macromolecular Therapeutics in Cancer Chemotherapy: Mechanism of Tumoritropic Accumulation of Proteins and the Antitumor Agent Smancs. *Cancer Res.* **1986**, *46*, 6387−6392.
(9) Yongdong, J.; Congxian, J.; Sheng-Wen, H.; O'Donnell, M.; Gao, X. Multifunctional Nanoparticles as Coupled Contrast Agents. *Nat. Commun.* **2010**, *1*, 41.
(10) Kim, J.; Park, S.; Lee, J. E.; Jin, S. M.; Lee, J. H.; Lee, I. S.; Yang, I.; Kim, J.-S.; Kim, S. K.; Cho, M.-H.; Hyeon, T. Designed Fabrication of Multifunctional Magnetic Gold Nanoshells and Their Application to Magnetic Resonance Imaging and Photothermal Therapy. *Angew. Chem.* **2006**, *118*, 7918−7922.
(11) Wang, F.; Chen, X.; Zhao, Z.; Tang, S.; Huang, X.; Lin, C.; Cai, C.; Zheng, N. Synthesis of Magnetic, Fluorescent and Mesoporous Core-Shell-Structured Nanoparticles for Imaging, Targeting and Photodynamic Therapy. *J. Mater. Chem.* **2011**, *21*, 11244−11252.
(12) Wang, M.; Gao, C.; He, L.; Lu, Q.; Zhang, J.; Tang, C.; Zorba, S.; Yin, Y. Magnetic Tuning of Plasmonic Excitation of Gold Nanorods. *J. Am. Chem. Soc.* **2013**, *135*, 15302−15305.
(13) Yu, H.; Chen, M.; Rice, P. M.; Wang, S. X.; White, R. L.; Sun, S. Dumbbell-like Bifunctional Au−Fe_3O_4 Nanoparticles. *Nano Lett.* **2005**, *5*, 379−382.
(14) Bhana, S.; Rai, B. K.; Mishra, S. R.; Wang, Y.; Huang, X. Synthesis and Properties of Near Infrared-Absorbing Magnetic-Optical Nanopins. *Nanoscale* **2012**, *4*, 4939−4942.
(15) Durgadas, C. V.; Sharma, C. P.; Sreenivasan, K. Fluorescent and Superparamagnetic Hybrid Quantum Clusters for Magnetic Separation and Imaging of Cancer Cells from Blood. *Nanoscale* **2011**, *3*, 4780−4787.
(16) Xu, Y.; Palchoudhury, S.; Qin, Y.; Macher, T.; Bao, Y. Make Conjugation Simple: A Facile Approach to Integrated Nanostructures. *Langmuir* **2012**, *28*, 8767−8772.
(17) Leung, K. C.-F.; Xuan, S.; Zhu, X.; Wang, D.; Chak, C.-P.; Lee, S.-F.; Ho, W. K. W.; Chung, B. C. T. Gold and Iron Oxide Hybrid Nanocomposite materials. *Chem. Rev.* **2012**, *41*, 1911−1928.
(18) Yu, M.; Zhou, C.; Liu, J.; Hankins, J. D.; Zheng, J. Luminescent Gold Nanoparticles with pH-Dependent Membrane Adsorption. *J. Am. Chem. Soc.* **2011**, *133*, 11014−11017.
(19) Kang, Y. S.; Risbud, S.; Rabolt, J. F.; Stroeve, P. Synthesis and Characterization of Nanometer-Size Fe_3O_4 and γ-Fe_2O_3 Particles. *Chem. Mater.* **1996**, *8*, 2209−2211.
(20) Laurent, S.; Forge, D.; Port, M.; Roch, A.; Robic, C.; Vander Elst, L.; Muller, R. N. Magnetic Iron Oxide Nanoparticles: Synthesis, Stabilization, Vectorization, Physicochemical Characterizations, and Biological Applications. *Chem. Rev.* **2008**, *108*, 2064−2110.
(21) Déry, J.-P.; Borra, E. F.; Ritcey, A. M. Ethylene Glycol Based Ferrofluid for the Fabrication of Magnetically Deformable Liquid Mirrors. *Chem. Mater.* **2008**, *20*, 6420−6426.
(22) Xu, Y.; Qin, Y.; Palchoudhury, S.; Bao, Y. Water-Soluble Iron Oxide Nanoparticles with High Stability and Selective Surface Functionality. *Langmuir* **2011**, *27*, 8990−8997.
(23) Karaagac, O.; Kockar, H.; Beyaz, S.; Tanrisever, T. A Simple Way to Synthesize Superparamagnetic Iron Oxide Nanoparticles in Air Atmosphere: Iron Ion Concentration Effect. *IEEE Trans. Magn.* **2010**, *46*, 3978−3983.
(24) Magde, D.; Wong, R.; Seybold, P. G. Fluorescence Quantum Yields and Their Relation to Lifetimes of Rhodamine 6G and Fluorescein in Nine Solvents: Improved Absolute Standards for Quantum Yields. *Photochem. Photobiol.* **2002**, *75*, 327−334.
(25) Chekina, N.; Horak, D.; Jendelova, P.; Trchova, M.; Benes, M. J.; Hruby, M.; Herynek, V.; Turnovcova, K.; Sykova, E. Fluorescent Magnetic Nanoparticles for Biomedical Applications. *J. Mater. Chem.* **2011**, *21*, 7630−7639.
(26) Fabbrizzi, L.; Licchelli, M.; Pallavicini, P.; Perotti, A.; Taglietti, A.; Sacchi, D. Fluorescent Sensors for Transition Metals Based on Electron-Transfer and Energy-Transfer Mechanisms. *Chem.—Eur. J.* **1996**, *2*, 75−82.
(27) Jares-Erijman, E. A. J.; Thomas, M. FRET Imaging. *Nat. Biotechnol.* **2003**, *21*, 1387−1395.
(28) Mori, K.; Kanai, S.; Hara, T.; Mizugaki, T.; Ebitani, K.; Jitsukawa, K.; Kaneda, K. Development of Ruthenium−Hydroxyapatite-Encapsulated Superparamagnetic γ-Fe_2O_3 Nanocrystallites as an Efficient Oxidation Catalyst by Molecular Oxygen. *Chem. Mater.* **2007**, *19*, 1249−1256.
(29) Zhang, Y.; Das, G. K.; Xu, R.; Yang Tan, T. T. Tb-doped Iron Oxide: Bifunctional Fluorescent and Magnetic Nanocrystals. *J. Mater. Chem.* **2009**, *19*, 3696−3703.
(30) Jun, Y.-w.; Seo, J.-w.; Cheon, J. Nanoscaling Laws of Magnetic Nanoparticles and Their Applicabilities in Biomedical Sciences. *Acc. Chem. Res.* **2008**, *41*, 179−189.
(31) Lee, N.; Hyeon, T. Designed Synthesis of Uniformly sized Iron Oxide Nanoparticles for Efficient Magnetic Resonance Imaging Contrast Agents. *Chem. Soc. Rev.* **2012**, *41*, 2575−2589.
(32) Tong, S.; Hou, S.; Zheng, Z.; Zhou, J.; Bao, G. Coating Optimization of Superparamagnetic Iron Oxide Nanoparticles for High T_2 Relaxivity. *Nano Lett.* **2010**, *10*, 4607−4613.
(33) Choi, J.-s.; Lee, J.-H.; Shin, T.-H.; Song, H.-T.; Kim, E. Y.; Cheon, J. Self-Confirming "AND" Logic Nanoparticles for Fault-Free MRI. *J. Am. Chem. Soc.* **2010**, *132*, 11015−11017.
(34) Jahnen-Dechent, W.; Ketteler, M. Magnesium Basics. *Clin. Kidney J.* **2012**, *5*, i3−i14.
(35) Izak-Nau, E.; Voetz, M.; Eiden, S.; Duschl, A.; Puntes, V. F. Altered Characteristics of Silica Nanoparticles in Bovine and Human Serum: The Importance of Nanomaterial Characterization Prior to Its Toxicological Evaluation. *Part. Fibre Toxicol.* **2013**, *10*, 1−12.